Mon. Not. R. Astron. Soc. **377,** 1520–1530 (2007) doi:10.1111/j.1365-2966.2007.11702.x

Evolutionary models for two hyper-iron-poor low-mass stars

Gregory J. Harris,⋆ Rachael Porter, A. E. Lynas-Gray and Jonathan Tennyson
Department of Physics and Astronomy, University College London, Gower Street, London WC1E 6BT

Accepted 2007 March 4. Received 2007 March 2; in original form 2006 December 15

ABSTRACT

The possible origin of two low-mass hyper-iron-poor (HIP) stars, HE0107-5240 and HE1327-2326 are investigated. The three scenarios tested are as follows. (i) The star forms metal free (Population III) and accretes metals throughout its lifetime. (ii) A Population III binary star system forms, and the lower mass star accretes metals from the higher mass star during its asymptotic giant branch phase. (iii) An HIP Population II star is formed and evolves with no further pollution. Using the NG-ELMS code, stellar evolution models of these three scenarios are computed and fitted to the observed colours. Models are computed at 0.8 and 0.7 $M_{\odot}$, and for several metal accretion rates.

It is not possible to unambiguously identify the origin, evolutionary stage or mass for either star with the present observational data. Our evolutionary models indicate that HE0107−5240 is either a red giant or a subgiant close to the base of the red giant branch. In line with the study of Aoki et al., HE1327−2326 is found to be either a main-sequence or a subgiant star. If HE1327−2326 is a main-sequence star the fits indicate that it must have a mass less than 0.8 $M_{\odot}$; if the star is assumed to have an age of around 12.5 Gyr it will have a mass closer to 0.7 $M_{\odot}$.

Main-sequence low-mass model Population III stars which have been polluted with metals are found to closely resemble Population II stars. However, the case is different for subgiants. The polluted and unpolluted Population III subgiants have luminosity up to twice that of a comparable Population II model. If HE1327−2326 is a subgiant, its distance is measured and if its mass can be reasonably well constrained, it should be possible to determine if it is a Population II or III star.

Key words: stars: abundances – stars: atmospheres – stars: carbon – stars: evolution – stars: low-mass, brown dwarfs.

1 INTRODUCTION

Conventional models of star formation in the early Universe suggest that only massive stars with correspondingly short lifetimes could be formed from the metal-free primordial gas (Nakamura & Umemura 2001; Bromm et al. 2003). However, there are claims that the initial mass function could be bimodal (Nakamura & Umemura 2001). In fact the two stars with the lowest iron abundances of any stars ever observed are almost certainly subsolar mass. HE0107−5240 has an iron abundance of [Fe/H] $= \sim -5.3$, a mass in the region of 0.8 $M_{\odot}$ and is thought to be a red giant (Christlieb et al. 2002; Weiss et al. 2004). HE1327−2326 is the most iron-deficient star ever discovered with an iron abundance of [Fe/H] ~ -5.4, 1/250 000 of the solar value (Aoki et al. 2006). This star is less evolved than HE0107−5240, but whether it is a subgiant or a dwarf star remains to be determined.

⋆E-mail: greg@theory.phys.ucl.ac.uk

These stars are the only two stars yet discovered with [Fe/H] < -5.0, but despite this they have carbon and nitrogen to iron ratios at least two orders of magnitude greater than the Sun Christlieb et al. (2004); Aoki et al. (2006); Collet, Asplund & Trampedach (2006). They have thus been classified as hyper-iron-poor (HIP) stars. Due to the extreme iron-deficient nature of these stars and the low metallicities, it is postulated that these stars may be samples from the first generation of stars that formed, Population III. However, as we show below, HIP stars evolve differently from completely metal-free stars. In this case their metal content should hold the key to their formation and evolution. In this paper we explore possible scenarios for forming the HIP stars as they are observed in the present epoch. For this we concentrate on the star HE1327−2326 as less work has been reported on this object than for HE0107−5240.

Naturally both HIP stars have aroused considerable interest since their detection. In particular Karlsson (2005, 2006) considered precisely the issue that concerns us here but did not address the important issue that the presence of metals significantly changes the evolution of the HIP star.

The evolution of stars with $Z = 10^{-10}$ and various masses was described by Cassisi, Castellani & Tornambe (1996). The main focus of this work is to test possible formation scenarios for HE1327−2326. The scenarios are also tested for HE0107−5240, but in less detail as they have already been studied by Suda et al. (2004) and Weiss et al. (2004).

2 BACKGROUND TO THE CALCULATIONS

The stellar evolution code NG-ELMS (Harris et al. 2007) was used to compute all the stellar evolutionary models reported here. NG-ELMS is a combination of the 1D low- and intermediate-mass stellar evolution code CESAM (Morel 1997) and a plane-parallel local thermodynamic equilibrium version of the stellar atmosphere code MARCS (Gustafsson et al. 1975). MARCS is used to compute a non-grey model atmosphere at run time to provide a surface boundary conditions for NG-ELMS. Spectral energy distributions and colour magnitudes are computed at run time. The subroutines which govern the equation of state, opacity and nuclear reactions in CESAM and MARCS have been rewritten. For high temperature opacities and equation of state we use the most recent OPAL data (Iglesias & Rogers 1996; Rogers & Nayfonov 2002). We use the NACRE nuclear reaction rates (Angulo et al. 1999) for the PP-chain, CNO cycle and triple alpha process. In line with our previous work Harris et al. (2007) we have adopted a value of the mixing-length parameter of $\alpha = 1.745$. The conductive opacities of Hubbard & Lampe (1969) are used. The diffusion of elements including metals is accounted for via the method of Michaud & Proffitt (1993).

The low-metallicity equation of state (LOMES) (Harris et al. 2004a,b, 2007) is used at low temperatures, this is an equation of state based upon the Saha equation. LOMES presently accounts for 15 elements: H, He, Li, C, N, O, Ne, Na, Mg, Al, Si, S, Ca, Ti, Fe and electrons. 136 species are accounted for including the first two ionization states and cations for each element, and many neutral molecules and molecular ions.

At high optical depths ($\tau > 15$) the diffusion approximation holds so that the Rosseland mean opacity is sufficient to compute the radiative temperature gradient. However, at low optical depths the diffusion approximation breaks down so that opacity cannot be treated as constant across all wavelengths. To overcome this problem we use a non-grey model atmosphere to provide the surface boundary condition, which requires monochromatic opacities over a wide range of frequencies.

To compute the monochromatic and Rosseland mean opacity at low temperatures we use an extended version of the low-temperature opacity subroutine from Harris et al. (2004a,b, 2006b). The various hydrogen and helium continuous opacity sources accounted for are listed in Harris et al. (2004a). In addition molecular line opacity for H_2O (Barber et al. 2006), HCN/HNC (Harris, Polyansky & Tennyson J. 2002; Harris et al. 2006a), CO (Goorvitch 1994), CN (Jørgensen & Larsson 1990), CH (Jørgensen et al. 1996), TiO (Plez 1998), OH (Kurucz 1995), NH (Kurucz 1995) and FeH (Dulick et al. 2003) is accounted for by a binned straight mean of the line opacity with Gaussian thermal Doppler line profiles. The straight mean is known to systematically over predict line opacity (Carbon 1974). However, for molecular bands which consist of many closely packed weak lines, the error is relatively small. For a few strong lines, such as atomic H lines, the systematic error can be very large. For atomic H and Li lines we use an opacity distribution function to partially overcome this problem. Atomic H and Li lines are taken from (1995, CD-ROM 1). For this present study other atomic metal lines have been neglected, none the less the present treatment of opacity is far superior to the use of the Rosseland mean opacity.

2.1 Physics of low-mass, zero-metallicity stars

On the main-sequence zero-metallicity low-mass stars tend to have a higher surface gravity and effective temperature than their counterparts with solar metallicity. This is because atomic line opacity at high temperature and electrons from ionized metals significantly increase opacity throughout the star. On the subgiant branch, however, zero-metallicity stars have a lower surface gravity and higher luminosity. This is due the absence of C, N and O in the core of the star so that the CNO cycle does not occur. The reduced rate of fusion due to the absence of the CNO cycle is compensated by a higher core temperature. The CNO cycle requires a mass fraction for C, N and O of only about 10^{-12}. The creation of small, but sufficient, quantities of C via the triple α process in red giants with core temperature above 5.5×10^7 K can occur. This gives rise to a 'CNO flash' (Schlattl et al. 2002) in stars above 0.9 $M_\odot$.

2.2 Abundance analyses of hyper-iron-poor stars

Most extremely metal deficient stars show abundance patterns which deviate significantly from solar metal abundance ratios. These may well provide us with insights into the early stages of chemical evolution in the Galaxy and Universe (Cayrel 2006). Many metal poor stars are enriched with carbon and most have over abundances of neutron capture elements (Norris, Ryan & Beers 1997). The HIP star HE1327−2326 has iron abundance of [Fe/H] = − 5.4 ± 0.2 (Frebel et al. 2005). Aoki et al. (2006) estimate the effective temperature of the star to be 6180 K with a surface gravity of log $(g) = 3.7$ for a subgiant or log $(g) = 4.5$ for a dwarf. There is a large over abundance of carbon in the star with [C/Fe] ≈ 4. There are higher than expected abundances of sodium, magnesium and aluminium, which are not observed for HE0107−5240. The abundances are [Na/Fe] ≈ 2.55, [Mg/Fe] ≈ 1.76 and [Al/Fe] ≈ 1.33 (Aoki et al. 2006). The origin of these elements is another issue surrounding the abundance pattern of HE1327−2326 that has not yet been fully understood. The abundance of nitrogen and oxygen also differs between the two HIP stars. HE1327−2326 has a much higher nitrogen abundance of [N/Fe] ≈ 4.56 and an oxygen abundance of [O/Fe] ≈ < 4.0, similar to carbon abundance (Aoki et al. 2006). The value of [N/Fe] and [O/Fe] is approximately 2.3 for HE0107−5240. Therefore when investigating scenarios for the origin of the star, the enrichment of carbon, nitrogen and oxygen over other elements is of great importance and must be accounted for.

During the course of this work Collet et al. (2006) published a differential 1D/3D model atmosphere abundance analysis study of HE0107−5240 and HE1327−2326. For HE1327−2326 their 3D model atmosphere uses fixed input parameters of $T_{\rm eff} = 6200$ K, $\log g = 4.34$ and a scaled solar composition of [Fe/H] = − 3. For HE0107−5240 these are $T_{\rm eff} = 5130$ K, $\log g = 2.2$ and [Fe/H] = − 3. The results for HE1327−2326 suggest that the abundance for Fe is ∼0.25 dex lower, and they suggest a downward revision for C, N and O abundances of up to an order of magnitude. For HE0107−5240 the suggested abundances of C, N and O are more than an order of magnitude smaller for the 3D case. These suggested downward revisions of metallicity are significantly larger than a similar 3D model atmosphere abundance analysis for the Sun (Asplund, Grevesse & Sauval 2005). This study revised downward the solar abundance of C, N and O by ∼0.2 dex, whilst the Fe abundance remains unchanged. The significant reduction in

the abundance of C, N and O estimated by Collet et al. (2006) will affect both the opacity and the equation of state of the gas and also the rate of the CNO cycle on the late main-sequence and subgiant branch. Most of our conclusions are drawn for the 1D abundance analyses of Christlieb et al. (2004); Bessell, Christlieb & Gustafsson (2004); Aoki et al. (2006), but we also comment on the implications of the 1D/3D differential study of Collet et al. (2006). Throughout this paper we use the solar abundances provided by Grevesse, Noels & Sauval (1996) as reference abundances.

2.3 Possible formation scenarios of HE1327−2326

The main formation scenarios as postulated by Suda et al. (2004) and Aoki et al. (2006) are as follows.

(i) An HIP Population II star forms with its present-day metallicity.

(ii) A hyper-metal-poor Population II star forms from gas polluted by the ejecta of a Population III supernova, further metals are then accreted on to the star over its lifetime.

(iii) An unpolluted Population III star accretes matter from a polluted cloud that surrounds the star.

(iv) An intermediate and low-mass Population III binary star pair forms. The secondary star accretes metals from the primary star during the primary stars asymptotic giant branch (AGB) phase. At the present epoch the primary star has become a white dwarf, so that only a low-mass star with an unusual metal composition is observed.

Several other formation scenarios have been postulated for HE0107−5240, but have since been ruled out. Among these is the possibility that the abundances of C and N were caused by self enhancement (Aoki et al. 2002). Weiss et al. (2004) have investigated flash-induced mixing (FIM), this is a process unique to metal free stars, in which the He flash enriches the envelope with C. This results in the star returning to the red giant branch, now fully enriched with C and N. However, their models have an effective temperature which is far too low, and C and N abundances which are two orders of magnitude too high. Christlieb et al. (2002) conclude that HE0107−5240 cannot be a post AGB star as the effective temperature is too low and the surface gravity too great. This is also true for HE1327−2326 and therefore self-enhancement is not considered here.

The large abundances of Sr with no Ba observed for HE1327−2326, supports the theory that the observed abundances may come from supernova remnants. The weak s-process is too inefficient at low metallicity to occur within HIP stars (Aoki et al. 2006). These elements are therefore likely to have been created by the r-process. Aoki et al. (2006) show how the r-process cannot be ruled out as the origin of Sr which may be created in Type II supernovae. This would support the scenario whereby the star formed in an already polluted cloud, or accreted metals from the ejecta of such a supernova.

3 METHOD

Models of star HE1327−2326 were tested for masses of $M_* = 0.8$ and $0.7\ M_\odot$. These masses were chosen to provide a realistic ages for models fit to the observed colours of HE1327−2326. NG-ELMS was modified to allow changes to the chemical abundance of the upper convective zone to simulate the accretion of metals from either the interstellar medium or from a binary companion. The mass of the accreted matter was assumed to be small so that any change in the mass of the star has not been accounted for. The change in the element abundances due to accretion is calculated at the same point as the change in abundances due to fusion and diffusion. The accreted material is assumed to homogeneously mix into the upper convective zone for each time-step. By using the metal abundance ratios of the accreted matter it is then straightforward to calculate the rate of change of each species due to accretion. For both the gradual and binary accretion scenarios metals are accreted with the metal abundance ratios of the dwarf fit of Aoki et al. (2006) for HE1327−2326 or the data of Christlieb et al. (2004), Bessell et al. (2004) for HE0107−5240. Only the accretion of C, N, O and Fe is studied in detail.

The averages of C, N and O abundances in iron-poor AGB star of initial mass 2–3 $M_\odot$ observed by Luck et al. (1993) are [C/Fe] = 2.85, [N/Fe] = 3.02 and [O/Fe] = 2.83. These metal abundance ratios are significantly different from the abundances observed in both HE1327−2326 and HE0107−5240, but do show a significant over abundance of C, N and O relative to Fe.

For the binary accretion scenario it was assumed that the primary star loses approximately 1.0 $M_\odot$ over 100 Myr. Some of this material is then accreted on to the secondary star over the 100-Myr period. The 100-Myr accretion period is far smaller than the 10 Gyr or more period over which the gradual accretion scenario occurs. So that the accretion rate for the binary star scenario will be far greater than for the gradual accretion scenario.

4 RESULTS

We have computed a range of models for both HE1327−2326 and HE0107−5240, to test the proposed formation and chemical enrichment scenarios. For each model we fitted the computed broadband colours, to the observed dereddened colours by minimizing the least-squares deviation. In general for each model fit to HE1327−2326, there are two minima in the least-squares deviation. These correspond to dwarf main-sequence and subgiant stars. There is only one least-squares minimum for each model fit to HE0107−5240, which correspond to either a red giant or a subgiant close to the base of the red giant branch.

4.1 Models and fits to the colours of HE1327−2326.

The first models to be computed were for metal free stars of 0.7 and 0.8 $M_\odot$ without accretion. These models are referred to as models A and B. The primordial element abundances used for the metal free models are quoted in Table 1. The metal mass fraction was set to a small finite value to avoid potential numerical problems. The adopted Population III hydrogen mass fraction was taken from the big bang nucleosynthesis calculations of Coc et al. (2004).

The initially polluted star scenario was tested by computing models of mass 0.7 and 0.8 $M_\odot$. For the initial chemical abundance ratios we used data from the element abundance analysis of Aoki et al. (2006). The dwarf abundances ratios were used for the 0.7-$M_\odot$ model and the subgiant abundance ratios for the 0.8-$M_\odot$ model. A slightly higher initial metallicity was used counter the metal depletion effect of element diffusion. The initial parameters are listed in Table 1, models C and D. The hydrogen mass fraction is very close to that of the Population III case. Model Z uses the metal abundances listed in Collet et al. (2006), for a 0.8-$M_\odot$ star.

Several models were computed to test the gradual accretion scenario. These models covered a range of accretion rates from 6×10^{-9} to $6 \times 10^{-12}\ M_\odot\ \mathrm{Myr}^{-1}$. The initial parameters for these models are listed in Table 1, models E to L.

Table 1. The initial parameters and accretion rates of metals for the models computed for HE1327−2326.

Model	Mass	X_0	log (Z_0)	Accretion rate ($M_\odot$ Myr^{-1})
A	0.7	0.7521	−12.621	0
B	0.8	0.7521	−12.621	0
C	0.7	0.7520	−3.4284	0
D	0.8	0.7520	−3.4284	0
E	0.7	0.7521	−12.621	6×10^{-9}
F	0.7	0.7521	−12.621	5×10^{-10}
G	0.7	0.7521	−12.621	6×10^{-11}
H	0.7	0.7521	−12.621	6×10^{-12}
I	0.8	0.7521	−12.621	6×10^{-9}
J	0.8	0.7521	−12.621	5×10^{-10}
K	0.8	0.7521	−12.621	6×10^{-11}
L	0.8	0.7521	−12.621	6×10^{-12}
M	0.7	0.7521	−12.621	10^{-7} binary
N	0.7	0.7521	−12.621	3.5×10^{-7} binary
O	0.7	0.7521	−12.621	7.5×10^{-7} binary
P	0.8	0.7521	−12.621	10^{-7} binary
Q	0.8	0.7521	−12.621	3.5×10^{-7} binary
R	0.8	0.7521	−12.621	7.5×10^{-7} binary
Z	0.8	0.7520	−4.6599	0

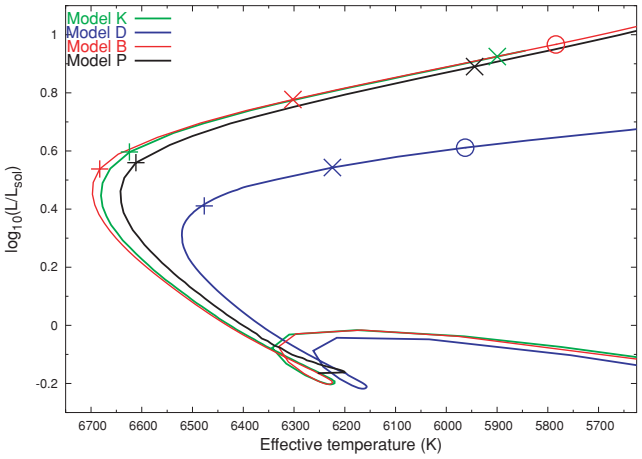

Figure 1. Evolutionary tracks on the Hertzsprung–Russell diagram of models B, D, K and P, which represent three different scenarios for a 0.8-$M_\odot$ star. Symbols are placed at ages of 11 Gyr (+), 11.75 Gyr (×) and 12 Gyr ($_\odot$).

Finally three accretion rates were used to compute models to test the binary accretion scenario. The accretion rates used are 10^{-7}, 3.5×10^{-7} and 7.5×10^{-7} $M_\odot$ Myr^{-1}. For each of the binary accretion models the accretion occurs for a period of 100 Myr, after which no further accretion of metals is allowed to occur. For the 0.8- and 0.7-$M_\odot$ models accretion starts at an age of 1.0 and 1.2 Gyr, respectively. At these ages both the 0.8- and 0.7-$M_\odot$ models are young main-sequence stars. The initial parameters and the accretion rate for the 100-Myr accretion period are listed in Table 1, models M to R.

The evolutionary tracks for models B, D, K and P are shown in Fig. 1. All these models are computed with an initial mass of 0.8 $M_\odot$ so the principal differences between these models is the metal content throughout the star. On the main-sequence fusion via the PP chain is the main energy production method. This means that the differences between the models on the main sequence are due to differences in the opacity and equation of state, which result from the different metal contents. Thus after the period of accretion the binary accreting star (model P), more closely resembles the initially polluted star (model D), but as metals diffuse from the convective envelope, its effective temperature moves closer that of the Population III case (model B). Towards the main-sequence turn-off and along the subgiant branch the CNO cycle starts to contribute significantly to energy production in the initially polluted star (model D). As the other models contain no C, N or O within their cores they do not undergo CNO cycle fusion, this results in a higher core temperature to maintain the fusion rate. Consequently for models B, K and P the main-sequence turn-off is at a higher effective temperature and a higher luminosity than for the initially polluted star (model D). Furthermore, models B, K and P have a significantly higher luminosity than model D along the subgiant branch, as a result they evolve more quickly along the subgiant branch.

We use the value for the interstellar extinction of $E(B-V) = 0.077$, which was adopted by Aoki et al. (2006) for HE1327−2326. The observed colours were dereddened by using the observed values of the optical and infrared extinction ratios listed in table 2 of Fitzpatrick (1999). Where a range of values are quoted we use the mid-point of the range. Aoki et al. (2006) quote three possible values for $E(B-V)$, we use the s.d. of these three values which is ∼0.02, to provide uncertainties on the interstellar extinction. This uncertainty, in turn provides errors on the fit of the evolutionary models and the resulting physical parameters.

Table 2 shows the colours, the physical parameters and their errors for each fit. Table 3 shows the surface metal abundance for each model. If the surface metal abundance for a given fit does not match the observed abundances within error or within one order of magnitude, we discount the fit and do not list it in Tables 2 and 3. The effective temperatures and surface gravities for each fit generally agree within error with those derived by Aoki et al. (2006).

It must be stressed that the quoted errors in Table 2 are due only to the uncertainty in interstellar extinction, and not any systematic errors in our models.

4.1.1 Population III models

For the Population III model B, the global best-fitting age is found to be at 11.86 ± 0.08 Gyr, corresponding to a subgiant star. The small apparent error on the age is due to the rapid evolution of effective temperature upon the subgiant branch. There is also a secondary minimum in the least-squares parameter, at an age of $10^{+1420}_{-0.5}$ Myr, which corresponds to a near zero-age main-sequence (ZAMS) star. The upper error bound upon this age is several orders of magnitude larger than the age of best fit, this is due to the slow evolution of effective temperature and the resulting colours along the main sequence. The lower error bound is considerable smaller, because the evolution of the effective temperature prior to the main sequence is very rapid. The relatively young age of all the 0.8-$M_\odot$ main-sequence fits, indicates that HE1327−2326 is very unlikely to be a 0.8-$M_\odot$ main-sequence star. Higher mass stars have a higher ZAMS $T_{\rm eff}$ which will not yield a main-sequence fit at all, thus if HE1327−2326 is a main-sequence star it is likely to have a mass less than 0.8 $M_\odot$.

For model A there are also two minima in the least-squares deviation. The first corresponds to an evolved main-sequence star at an age of 12.8^{+5}_{-3} Gyr. The large error is due to the proximity of the star to the main-sequence turn-off, which results in the upper value of the extinction coefficient [$E(V-B) = 0.097$] giving a fit to a subgiant star. The second minimum corresponds to a subgiant star

Table 2. Colour indices and physical parameters of the best-fitting ages for each model for HE1327−2326, and the observed colours of HE1327−2326. The dereddened observed colours and the effective temperature, surface gravity and distance estimated by Aoki et al. (2006), denoted [1], are also listed. Here σ denotes s.d. of the fit to the observed colours.

Model	Age (Myr)	$T_{\rm eff}$ (K)	log $(L/{\rm L}_\odot)$	log $(R/{\rm R}_\odot)$	log g	$U-B$	$B-V$	$V-R$	$V-K$	$R-I$	$I-J$	$J-H$	$H-K$	V	Distance (pc)	σ
Observed[a]						−0.283	0.404	0.264	1.337	0.294	0.449	0.262	0.068	13.332[b]		
[1]		6180			3.7/4.5										1400/470	
A	12772^{+5000}_{-3000}	6133 ± 120	−0.10 ± 0.5	−0.10 ± 0.2	4.49 ± 0.4	−0.368	0.513	0.314	1.318	0.333	0.349	0.291	0.032	5.04 ± 1.2	456 ± 200	0.071
A	18000 ± 400	6110 ± 100	0.47 ± 0.1	0.19 ± 0.07	3.91 ± 0.1	−0.340	0.510	0.310	1.325	0.332	0.355	0.298	0.030	3.61 ± 0.03	880 ± 100	0.065
B	$10^{+1420}_{-0.5}$	6120 ± 150	−0.02 ± 0.13	−0.06 ± 0.09	4.46 ± 0.17	−0.366	0.516	0.316	1.327	0.335	0.351	0.292	0.033	4.84 ± 0.32	500 ± 80	0.071
B	11860 ± 80	6110 ± 130	0.85 ± 0.05	0.38 ± 0.04	3.59 ± 0.09	−0.319	0.504	0.306	1.317	0.329	0.356	0.300	0.028	2.67 ± 0.12	1360 ± 73	0.061
C	14630 ± 3400	6142 ± 120	−0.02 ± 0.2	−0.07 ± 0.07	4.41 ± 0.2	−0.358	0.516	0.311	1.310	0.331	0.347	0.290	0.031	4.85 ± 0.05	497 ± 100	0.071
C	17770 ± 600	6100 ± 90	0.28 ± 0.06	0.09 ± 0.06	4.10 ± 0.01	−0.343	0.518	0.313	1.329	0.334	0.355	0.297	0.031	4.09 ± 0.3	707 ± 80	0.068
D	160^{+2400}_{-150}	6150 ± 100	−0.21 ± 0.2	−0.16 ± 0.1	4.66 ± 0.2	−0.348	0.522	0.313	1.306	0.332	0.344	0.286	0.031	5.32 ± 0.04	400 ± 70	0.071
D	11590 ± 100	6089 ± 130	0.57 ± 0.03	0.24 ± 0.07	3.86 ± 0.07	−0.321	0.518	0.312	1.333	0.334	0.358	0.300	0.030	3.35 ± 0.08	990 ± 40	0.065
E	15640^{+250}_{-2000}	6010 ± 25	0.04 ± 0.13	−0.01 ± 0.06	4.31 ± 0.12	−0.290	0.583	0.322	1.361	0.342	0.363	0.301	0.033	4.68 ± 0.3	540 ± 70	0.083
F	12992 ± 4400	6128 ± 110	−0.09 ± 0.4	−0.10 ± 0.2	4.48 ± 0.4	−0.360	0.519	0.314	1.318	0.333	0.349	0.291	0.032	5.01 ± 1	461 ± 170	0.071
F	17972 ± 600	6089 ± 100	0.46 ± 0.1	0.18 ± 0.1	3.92 ± 0.2	−0.318	0.529	0.312	1.328	0.333	0.356	0.298	0.030	3.65 ± 0.36	865 ± 170	0.068
G	17994 ± 420	6110 ± 110	0.47 ± 0.1	0.18 ± 0.07	3.92 ± 0.1	−0.337	0.512	0.310	1.323	0.332	0.355	0.297	0.030	3.63 ± 0.3	873 ± 110	0.066
H	18000 ± 400	6111 ± 100	0.47 ± 0.1	0.19 ± 0.07	3.91 ± 0.1	−0.340	0.510	0.310	1.324	0.332	0.355	0.298	0.030	3.62 ± 0.3	877 ± 110	0.065
I	$10^{+2500}_{-0.5}$	6120 ± 140	−0.02 ± 0.1	−0.06 ± 0.07	4.46 ± 0.14	−0.366	0.516	0.316	1.327	0.335	0.351	0.292	0.033	4.84 ± 0.25	500 ± 60	0.071
J	105^{+550}_{-95}	6220 ± 150	−0.20 ± 0.2	−0.16 ± 0.1	4.66 ± 0.2	−0.383	0.501	0.306	1.273	0.324	0.334	0.280	0.029	5.28 ± 0.5	410 ± 70	0.077
K	11660 ± 60	6080 ± 110	0.86 ± 0.04	0.39 ± 0.04	3.57 ± 0.08	−0.295	0.526	0.308	1.328	0.331	0.359	0.302	0.028	2.64 ± 0.1	1375 ± 60	0.065
L	11870 ± 80	6110 ± 130	0.85 ± 0.05	0.37 ± 0.04	3.59 ± 0.1	−0.318	0.504	0.306	1.317	0.329	0.356	0.300	0.028	2.67 ± 0.12	1360 ± 80	0.061
M	13462 ± 3700	6140 ± 130	−0.07 ± 0.3	−0.09 ± 0.1	4.46 ± 0.3	−0.364	0.513	0.312	1.311	0.332	0.347	0.289	0.031	4.95 ± 0.7	474 ± 130	0.071
M	18042 ± 600	6085 ± 120	0.47 ± 0.1	0.19 ± 0.1	3.90 ± 0.2	−0.336	0.516	0.313	1.338	0.335	0.359	0.300	0.031	3.61 ± 0.4	880 ± 150	0.066
N	14462 ± 3600	6150 ± 120	−0.01 ± 0.2	−0.06 ± 0.07	4.40 ± 0.1	−0.354	0.518	0.311	1.307	0.331	0.346	0.289	0.031	4.82 ± 0.4	504 ± 140	0.071
N	17862 ± 600	6111 ± 110	0.39 ± 12	0.15 ± 0.07	4.00 ± 0.1	−0.335	0.517	0.311	1.322	0.332	0.353	0.296	0.030	3.81 ± 0.3	802 ± 100	0.067
O	17602 ± 740	6096 ± 90	0.30 ± 0.1	0.10 ± 0.08	4.08 ± 0.2	−0.327	0.529	0.313	1.327	0.333	0.354	0.296	0.031	4.04 ± 0.3	723 ± 100	0.069
P	1450 ± 400	6210 ± 30	−0.15 ± 0.02	−0.14 ± 0.005	4.62 ± 0.01	−0.328	0.522	0.304	1.265	0.322	0.332	0.279	0.028	5.17 ± 0.05	430 ± 10	0.075
P	11680 ± 80	6080 ± 130	0.84 ± 0.05	0.38 ± 0.4	3.60 ± 0.09	−0.312	0.512	0.309	1.334	0.333	0.361	0.303	0.029	2.69 ± 0.13	1340 ± 80	0.062
Q	2630 ± 800	6200 ± 50	−0.12 ± 0.03	−0.12 ± 0.01	4.58 ± 0.02	−0.321	0.526	0.304	1.268	0.323	0.333	0.280	0.028	5.08 ± 0.007	450 ± 20	0.075
Q	11670 ± 100	6110 ± 100	0.77 ± 0.05	0.33 ± 0.04	3.67 ± 0.08	−0.306	0.513	0.307	1.32	0.329	0.355	0.299	0.028	2.87 ± 0.1	1240 ± 70	0.063
R	11560 ± 200	6110 ± 90	0.65 ± 0.07	0.28 ± 0.05	3.79 ± 0.1	−0.293	0.523	0.307	1.313	0.329	0.352	0.296	0.028	3.17 ± 0.2	1080 ± 90	0.065
Z	124^{+400}_{-100}	6216 ± 140	−0.20 ± 0.2	−0.16 ± 0.1	4.66 ± 0.2	−0.38	0.502	0.306	1.274	0.325	0.335	0.280	0.029	5.28 ± 0.4	408±70	0.076
Z	11500 ± 45	6109 ± 110	0.72 ± 0.03	0.31 ± 0.03	3.72 ± 0.05	−0.328	0.508	0.308	1.322	0.331	0.356	0.299	0.029	3.00 ± 0.06	1170 ± 30	0.063

[a] Dereddened observed colours from Aoki et al. (2006). [b] The observed apparent visual magnitude.

Table 3. The metal abundance ratios relative to the solar values (Grevesse et al. 1996) for the fits to HE1327−2326. The results of 1D and 3D abundance analysis are also listed. MS denotes a main-sequence fit, SG denotes a subgiant fit and TO the assumption that HE1327−2326 is a main-sequence turn-off star.

Model	Fit	[C/H]	[N/H]	[O/H]	[Fe/H]
1D[a]	MS	−1.76	−1.64	< − 2.17	−5.60
1D[b]	SG	−1.56	−1.14	< − 1.87	−5.61
3D[c]	TO	−2.3	−2.0	−2.8	−5.9
C	MS	-1.59 ± 0.03	-1.47 ± 0.03	-1.70 ± 0.03	-5.53 ± 0.03
C	SG	-1.62 ± 0.04	-1.49 ± 0.04	-1.72 ± 0.04	-5.56 ± 0.04
D	MS	-1.38 ± 0.03	-0.99 ± 0.03	-1.82 ± 0.03	-5.32 ± 0.03
D	SG	-1.52 ± 0.03	-1.13 ± 0.03	-1.96 ± 0.03	-5.44 ± 0.03
E	MS	-0.56 ± 0.1	-0.14 ± 0.1	-0.87 ± 0.1	-4.72 ± 0.1
F	MS	-1.66 ± 0.6	-1.54 ± 0.6	-1.77 ± 0.6	-5.61 ± 0.6
F	SG	-1.04 ± 0.07	-0.92 ± 0.07	-1.15 ± 0.07	-4.99 ± 0.07
G	SG	-1.87 ± 0.07	-1.75 ± 0.07	-1.98 ± 0.07	-5.82 ± 0.07
H	SG	-2.89 ± 0.1	-2.77 ± 0.1	-3.00 ± 0.1	-6.84 ± 0.1
I	MS	-3.29 ± 2.5	-2.87 ± 2.5	-3.60 ± 2.5	-7.45 ± 2.5
J	MS	-2.80 ± 1.8	-2.68 ± 1.8	-2.91 ± 1.8	-6.75 ± 1.8
K	SG	-0.59 ± 0.09	-0.47 ± 0.09	-0.69 ± 0.1	-4.51 ± 0.1
L	SG	-2.42 ± 0.6	-2.00 ± 0.6	-2.73 ± 0.6	-6.57 ± 0.6
M	MS	-1.95 ± 0.04	-1.83 ± 0.04	-2.06 ± 0.04	-5.89 ± 0.04
M	SG	-2.01 ± 0.01	-1.88 ± 0.01	-2.11 ± 0.01	-5.94 ± 0.01
N	MS	-1.40 ± 0.03	-1.28 ± 0.03	-1.51 ± 0.03	-5.34 ± 0.03
N	SG	-1.44 ± 0.01	-1.32 ± 0.01	-1.55 ± 0.01	-5.38 ± 0.01
O	SG	-1.09 ± 0.01	-0.969 ± 0.01	-1.20 ± 0.01	-5.03 ± 0.01
P	MS	-0.86 ± 0.15	-0.47 ± 0.15	-1.30 ± 0.15	-4.79 ± 0.15
P	SG	-1.95 ± 0.1	-1.56 ± 0.1	-1.24 ± 0.1	-5.84 ± 0.1
Q	MS	-0.80 ± 15	-4.09 ± 15	-1.24 ± 15	-4.74 ± 0.15
Q	SG	-1.36 ± 0.05	-0.96 ± 0.04	-1.79 ± 0.04	-5.26 ± 0.04
R	SG	-0.95 ± 0.01	-0.56 ± 0.01	-1.38 ± 0.01	-4.86 ± 0.01
Z	MS	-2.60 ± 0.01	-2.22 ± 0.01	-3.08 ± 0.01	-5.96 ± 0.01
Z	SG	-2.78 ± 0.04	-2.39 ± 0.04	-3.25 ± 0.04	-6.12 ± 0.04

[a]From Aoki et al. (2006), the mean of quoted abundance values. [b]From Aoki et al. (2006), the mean of quoted abundance values. [c]From Collet et al. (2006).

at an age of 18 ± 0.4 Gyr. The age of the subgiant fit for all the 0.7-$M_\odot$ models is significantly larger than the *Wilkinson Microwave Anisotropy Probe* (*WMAP*) age of the Universe. Therefore it is unlikely that HE1327−2326 has a mass smaller than 0.7 $M_\odot$ if it is a subgiant.

4.1.2 Initially polluted models

The main-sequence fits for models C and D have s.d. in the fit of the observed colours of only 10 per cent greater than the subgiant fits, so they cannot be discounted on grounds of being a poorer fit to the observed colours alone. The main-sequence fit of model D is at an age of 160^{+2400}_{-150} Myr, its young age implies this fit is unlikely to be the true case for HE1327−2326. However, model C results in an older main-sequence age of 14.6 ± 3.4 Gyr, although older than the model A main-sequence fit it is within error bounds of the *WMAP* age of the Universe.

The fits for a subgiant star with and without metals have significantly different derived luminosities and distances. For example the distance of the metal free model B subgiant fit is 1.36 ± 0.073 kpc and the distance of the polluted model D fit is 0.99 ± 0.04 kpc. This again is due to the absence of fusion via the CNO cycle in the metal-free subgiant.

The lower metallicity, model Z also has a main-sequence and a subgiant fit. The fit for the main sequence is mostly indistinguishable from the main-sequence fits of models B and D. However, the subgiant fit for model Z takes values of luminosity, surface gravity and absolute *V* magnitude halfway between the subgiant fits of models B and D. The reason for this is that the reduced abundance of C, N and O, result in a reduced rate of fusion via the CNO cycle. Core temperature, density and percentage energy generation via the CNO cycle for models B, D, Z at the age of best fit are listed in Table 4. The core temperature and density of model Z are higher than that of model D, by around 20 per cent, but the core temperature of model Z is still 10 MK less than that of model B. Conversely the core density of model Z is closer to that of model B, than model D. Overall, reducing the abundances, by approximately an order of magnitude, from those given by Aoki et al. (2006) to those suggested by Collet et al. (2006), results in a fit for a subgiant roughly halfway between that of model B and model D. This suggests that if HE1327−2326 is indeed a subgiant then an accurate determination of distance and mass could provide vital information on the abundance of C, N and O in the star.

Table 4. Core temperature and density, and percentage energy generation via the CNO cycle at age of best-fitting subgiant, for models B, D and Z.

Model	ρ_c (kg cm^{-3})	T_c (MK)	CNO (per cent)
B	14.2	39.5	0
D	7.33	25.0	52
Z	11.9	29.2	42

4.1.3 Gradual accretion models

The gradual accretion scenario was studied using several accretion rates and at masses of 0.8 and 0.7 $M_\odot$. The models computed for 0.7 $M_\odot$ are E to H, and those for 0.8 $M_\odot$ are I to L. In general each model results in a main-sequence and a subgiant fit, however the fits which have surface metal abundances which deviate from the Aoki et al. (2006) dwarf fit abundances for HE1327−2326 by more than an order of magnitude are discounted and not listed.

For each of these models the metallicity rises along the main sequence, this increases the atmospheric opacity and acts to cool the effective temperature. Thus at main-sequence turn-off models with higher accretion rates have redder colours than those with lower accretion rates. This results in main-sequence fits with significantly different ages for models E and F. The model E main-sequence fit is near main-sequence turn-off, whilst at best-fitting model F is younger than model E and has a higher $T_{\rm eff}$. Model F has several billion years of its main-sequence lifetime remaining. The surface metallicities of model F far more closely match the observed metallicities of HE1327−2326, it is model F that therefore provides the most realistic main-sequence fit for a 0.7-$M_\odot$ gradual accretion model.

The main-sequence fits for a 0.8-$M_\odot$ model are I and J. These fits correspond to either a late pre-main-sequence or early main-sequence star. The large upper errors are a result of the slow evolution of effective temperature on the main sequence whilst the small lower error is a result of the rapid pre-main-sequence evolution. Both the models have large errors on metallicity, this is due to the large relative errors on age. The observed metal abundances of HE1327−2326 falls easily within the large uncertainties in surface element abundance which all these models have. Again the very young ages of these main-sequence fits indicate that if HE1327−2326 is a main-sequence star it is likely to have mass less than 0.8 $M_\odot$.

Models F, G and H provide fits for the 0.7-$M_\odot$ subgiant case, each has a very similar age, $T_{\rm eff}$ and luminosity. Model G provides the closest match to the observed metal abundance ratios of HE1327−2326. As with the subgiant fits of models A and C the age of these models is ∼18 Gyr, which is considerably larger than the *WMAP* age of the Universe. So the subgiant fits of models F, G and H can be discounted.

Models K and L provide fits for the subgiant branch with a mass of 0.8 $M_\odot$. Both fits have an age of 11.9 Gyr. Neither model K nor L provide good fits to the surface element abundance, K giving an metal abundance which is too high and L an element abundance which is too low. An accretion rate which results in a better fit to observed abundances is likely to lie between 6×10^{-11} and 6×10^{-12} $M_\odot$ Myr^{-1}.

The evolutionary tracks of the gradual accretion models move from the Population III case on the early main sequence towards the HIP Population II case. However, on the subgiant branch for a given luminosity the gradual accretion models bear a closer resemblance to a Population III subgiant. The luminosity is considerably higher for a given $T_{\rm eff}$ than the polluted metallicity case. None of the accreted C, N and O has had sufficient time to diffuse in significant quantities into the radiative interiors of the star.

4.1.4 Binary accretion models

Models M to R have been computed to address the binary accretion scenario, for masses of 0.8 and 0.7 $M_\odot$. The main-sequence fits are M and N for the 0.7-$M_\odot$ case and P and Q for the 0.8-$M_\odot$ case. The main-sequence fit provided by model M is slightly younger than that from model N, due to its lower abundance of metals. Model N provides the best agreement with the observed metallicities of HE1327−2326 for the 0.7-$M_\odot$ case, and model P for the 0.8-$M_\odot$ case. Again the 0.7-$M_\odot$ models provide the most realistic main-sequence age for HE1327−2326.

All the binary accretion models M to R provide fits for a subgiant star. Models N and Q with an accretion rate of 3.5×10^{-7} $M_\odot$ Myr^{-1}, provide the best agreements with the observed abundances for 0.7- and 0.8-$M_\odot$ models, respectively. As with all the other 0.7-$M_\odot$ subgiant fits model N has an age of ∼18 Gyr, which is significantly larger than the age of the Universe.

4.2 Best fits for HE0107−5240

The star HE0107−5240 has colours which are consistent with a red giant. As red giant stars transport energy via superadiabatic convection in their extensive envelopes, the effective temperature of model red giant is heavily dependent upon the value of the mixing-length parameter. This makes the fitting of red giant colours highly uncertain. With this in mind three models with mass of 0.8 $M_\odot$ have been computed for HE0107−5240 one for Population III (model [a]), one for HIP Population II star with no accretion (model [b]) and finally a Population III star with a constant gradual accretion rate of 2.3×10^{-12} $M_\odot$ Myr^{-1} (model [c]). Model [c] accretes at a constant rate throughout its entire lifetime. The chemical composition of the accreted gas is that of HE0107−5240 given by Christlieb et al. (2004) and Bessell et al. (2004).

The observed colours have been dereddened by using the mean of the two extinction coefficients quoted by Christlieb et al. (2004), which are $E(B-V) = 0.013$ and $E(B-V) = 0.00$. The two extinction coefficients provide an error in the observed colour indices from which errors in the fit result. The results of the fits are given in Tables 5 and 6. All the fits correspond to stars on the lower part of the red giant branch. Age, luminosity, effective temperature, radius and surface gravity of models [a] and [c] agree closely with each other. This is because the surface metallicity of model [c] is three orders of magnitude lower than the metallicity of HE0107−5240 determined by Christlieb et al. (2004), Bessell et al. (2004). The best fits of models [a] and [b] differ in age by 0.4 Gyr and model [b] has a much lower luminosity.

Fig. 2 shows the late subgiant branch and base of the red giant branch for models [a] and [b]. The core temperatures of model [a] at time of best fit is 5.79×10^7 K, the core density is 2.19×10^5 g cm^{-3}, 99 per cent of the energy that is released is via the PP-chain, with the remainder from gravitational contraction of the core. The total mass fractions of the C, N, O elements in the core is 1.34×10^{-9}, these have been created via a small amount of triple alpha fusion. The core temperatures of model [b] at time of best fit is 3.24×10^7 K, the core density is 9.56×10^4 g cm^{-3}, 87 per cent of the energy that is released is from the CNO cycle, with 12 per cent from the PP-chain and the remainder from the gravitational contraction of the core It is clear that due to the absence of a CNO cycle, model [a] is significantly more luminous than model [b] across the subgiant branch. The base of the red giant branch is also at a higher luminosity than for model [b].

The creation of the CNO elements in model [a] results in a weak 'CNO flash' (Schlattl et al. 2002) at an age of 12.16 Gyr and a core temperature of 5.9×10^7 K. Prior to the CNO flash the hydrogen mass fraction is $\sim 10^{-5}$, the CNO flash reduces this to less than 10^{-12} within 20 Myr. The injection energy into the core causes the core to expand and cool slightly. However, these small changes in the

Table 5. Colour indices and physical parameters of the best-fitting ages for each model for HE0107−5240, and the observed colours of HE0107−5240. Also listed are the effective temperature determinations of Christlieb et al. (2004), denoted [1], and the FIM and Population II.5 models of Weiss et al. (2004), denoted [2] and [3], respectively. Here σ denotes s.d. of the fit to the observed colours.

Model	Age (Myr)	$T_{\rm eff}$ (K)	$\log(L/L_\odot)$	$\log(R/R_\odot)$	$\log g$	$U-B$	$B-V$	$V-R$	$V-K$	$R-I$	$I-J$	$J-H$	$H-K$	V	Distance (pc)	σ
Observed[a]							0.69	0.44	1.94	0.44	0.60	0.47	−0.01	15.17[b]		
[1]		5160 ± 200			2.2 ± 0.3											
[2]	13100	5026	1.8	–	2.3											
[3]	–	4520	1.7	–	2.3											
[a]	12300 ± 20	5180 ± 30	1.40 ± 0.04	0.80 ± 0.03	2.75 ± 0.05	−0.140	0.704	0.432	1.928	0.457	0.538	0.427	0.074	1.28 ± 0.1	2570 ± 120	0.047
[b]	11900 ± 60	5210 ± 30	1.10 ± 0.05	0.64 ± 0.03	3.06 ± 0.01	−0.213	0.797	0.425	1.883	0.450	0.522	0.413	0.073	2.05 ± 0.1	1810 ± 120	0.071
[c]	12300 ± 16	5175 ± 20	1.41 ± 0.04	0.80 ± 0.02	2.74 ± 0.05	−0.140	0.704	0.433	1.929	0.457	0.538	0.428	0.074	1.29 ± 0.1	2580 ± 120	0.047

[a]Dereddened observed colours from Christlieb et al. (2004). [b]The observed apparent visual magnitude.

core induce no appreciable change in the luminosity and effective temperature in a star of mass less than about 0.9 $M_\odot$.

The exact positions of HE0107−5240 on the red giant branch is subject to a high degree of uncertainty due to the inherent uncertainties in the treatment of superadiabatic convection in mixing-length theory. A model calculated with a slightly different value of the mixing-length parameter will result in a fit with significantly different position on the red giant branch. A parallax distance measurement to HE0107−5240 and thus the absolute magnitude would help to tie down the position of the star on the red giant branch.

Model [c] indicates that an accretion rate of around three orders of magnitude larger than the adopted value is required to reproduce the observed surface metal abundances. This would result in a significantly higher accretion rate than the one used for the models for HE1327−2326. The main reason for this is that red giants have significantly larger convective zones than subgiants and main-sequence stars. Thus, to induce the same change in surface metallicity a larger fraction of a red giant would have to have been polluted than for a subgiant or main-sequence star.

5 DISCUSSION

The best-fitting models for main-sequence models for HE1327−2326 are C, F and N, and for the subgiant fits are D, K/L and Q. These models most closely match the colours and metallicities of HE1327−2326 and also show realistic ages. The total mass accreted is a function of only the age of the model. However, the surface metal abundances are affected not only by the total mass of accreted matter, but also by the evolution of the convective envelope and the microscopic diffusion of metals. The affects of accretion, and the convective and microscopic diffusion of metals can be seen in Figs 3 and 4, which show the evolution of the surface carbon abundance. The short burst of accretion in the binary accreting models N and P occurs shortly after an age of 1 Gyr. Over the course of the main-sequence, microscopic diffusion depletes metals from the surface of models N and P and the non-accreting models C and D. In contrast for models F and L, the surface metal enrichment rate due to accretion is always greater than the microscopic diffusion depletion rate. The surface abundance of metals in the gradual accretion models F and L increases more rapidly as the convective envelope shrinks during the course of the main sequence. For the 0.8-$M_\odot$ models, the mass of the convective envelope reaches a minimum on the early part of the subgiant branch, at an age of ∼11 Gyr. At this point both the level and the rate of metal enrichment for model L, reach their maximum. In the latter part of the subgiant phase all the models develop deep convective envelopes. At this stage the deep convective envelope mixes the metal rich surface gas with metal deficient gas from the stellar interior, decreasing the surface metal abundance of models F and L. In contrast for models N and P, the gas immediately below the convective envelope has become enriched with metals by diffusion from the surface. When the surface gas is mixed with this metal rich gas, the surface metallicity temporarily increases. This temporary metal enrichment does not occur for model F and L, because continual accretion ensures that the gas immediately below the convective envelope always has a lower metallicity than the surface.

The accretion rates used here only account for the accretion of metals. In reality the metals are only likely to account for 1 or 2 per cent of the matter accreted, the rest being hydrogen and helium. This means that to reach the observed metallicity of HE1327−2326 model F has to accurate about $6.5 \times 10^{-4}\,M_\odot$ from interstellar gas

Table 6. The surface metal abundance ratios relative to the solar values (Grevesse et al. 1996) for each of the model fits to HE0107−5240. Also listed are the 1D and 3D abundance analysis and FIM and Population II.5 evolution models of Weiss et al. (2004).

Model	[C/H]	[N/H]	[O/H]	[Fe/H]
1D[a]	−1.59	−2.90	−3.25	−5.39
3D[b]	−2.8	−4.2	−3.8	−5.6
Population II.5[c]	−1.7	−2.4	−1.3	−5.3
FIM[c]	0.7	0.9	−2.7	−5.3
[b]	−1.46 ± 0.004	−2.89 ± 0.003	−3.06 ± 0.003	−5.38 ± 0.003
[c]	−4.33 ± 0.02	−5.76 ± 0.02	−5.93 ± 0.02	−8.24 ± 0.02

[a]From Christlieb et al. (2004) and Bessell et al. (2004); [b]Collet et al. (2006); [c]Weiss et al. (2004).

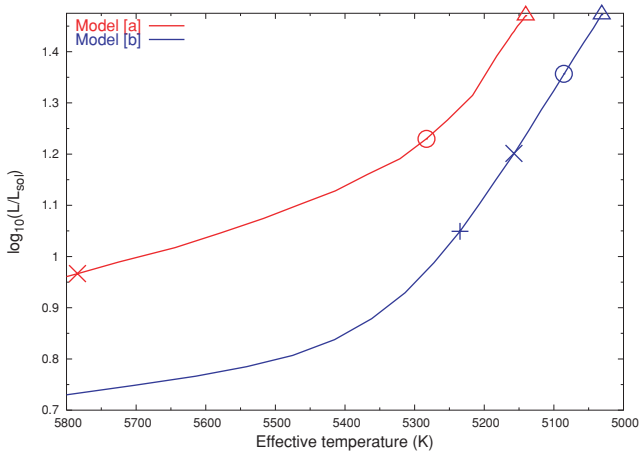

Figure 2. Evolutionary tracks of models [a] and [b], which represent the initially polluted and Population III scenarios for a 0.8-$M_\odot$ models of HE0107−5240. Symbols are placed at ages of 11.8 Gyr (+), 12 Gyr (×), 12.2 Gyr ($\odot$) and 13.32 Gyr (△).

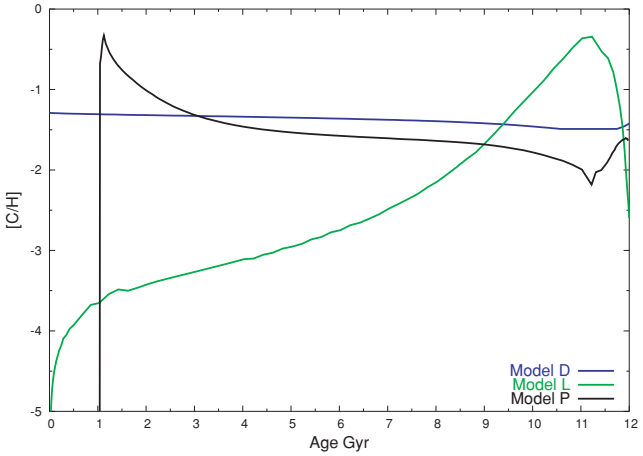

Figure 3. The evolution of the surface abundance of carbon in three representative models of 0.8 $M_\odot$.

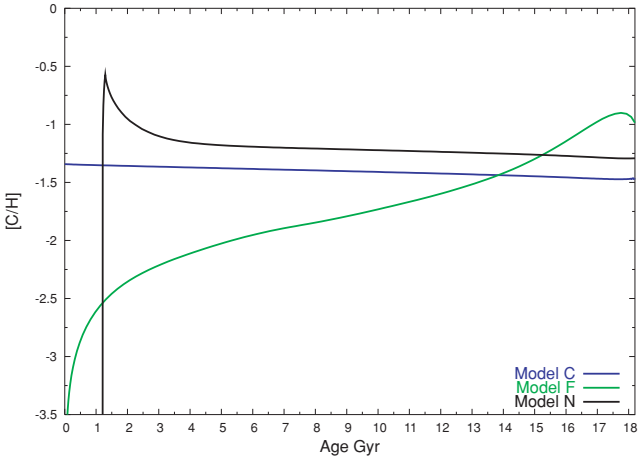

Figure 4. The evolution of the surface abundance of carbon in three representative models of 0.7 $M_\odot$.

whilst model N accretes 3.5×10^{-3} $M_\odot$ from a companion star. It is conceivable that 3.5×10^{-3} $M_\odot$ could be accreted from a companion star, but an accretion of 6.5×10^{-4} $M_\odot$ of interstellar gas is unrealistically large. Indeed, Suda et al. (2004) estimate that a 0.8-$M_\odot$ star of an age of 10 Gyr would accrete 2.6×10^{-8} $M_\odot$. Models K and L accrete 7×10^{-5} and 7×10^{-6} $M_\odot$, respectively. This is still two to three orders of magnitude higher than the accretion estimate of Suda et al. (2004). If the corrections to the metal abundances suggested by Collet et al. (2006) are correct then the metallicity is reduced by around an order of magnitude. However, this would still require one to two orders of magnitude more accretion from the interstellar medium than allowed for by the estimate of Suda et al. (2004).

To increase the accretion rate of interstellar gas HE1327−2326 would need to spend a considerable length of time accreting from a dense cloud of gas. A possible, but unlikely, alternative is that of a Population III star colliding with a Population I or II stellar system resulting in mass transfer between stars or the absorption of a planet. Stellar encounters are not that unusual, but direct collisions are likely to be extremely rare. None the less this scenario merits future investigation.

The accretion of metals can allow a Population III main-sequence star to have effective temperature and luminosity close to that of a comparable HIP Population II star. On the main sequence the PP-chain is the dominant form of fusion for a low-mass star. However, fusion via the CNO cycle is important on the subgiant and giant branches. For Population III stars, a higher core temperature is required to sustain fusion rates via the PP-chain. This gives rise to a luminosity about twice that of Population II subgiant stars. This luminosity difference may allow HE1327−2326 to be definitively identified as a Population II or III star. However, the luminosity of the subgiant branch at a given effective temperature is also a function of mass and metallicity. This would require the mass of HE1327−2326 to be constrained, so that the luminosity of an HIP Population II model at the upper limit of mass is smaller than the luminosity of a polluted Population III model at the lower mass limit.

A Population III subgiant of 0.75 $M_\odot$ and effective temperature of $\sim$6100 K has a luminosity $\log(L/L_\odot) = 0.681$ (Harris et al. 2007). This is just below the mid-point in luminosity between model D and B. The mass of HE1327−2326 will therefore need to constrained to better than 0.05 $M_\odot$ in order to determine if HE1327−2326 is a Population II or III star.

The corrections suggested by Collet et al. (2006) to the metallicity also significantly affect the luminosity of the subgiant branch. Although the abundances of C, N and O are reduced by around an order of magnitude in model Z, the CNO cycle remains very important. This is due to the very strong power law temperature dependence of the reaction rates of the CNO cycle, a reduction in the abundance of C, N and O can be countered by a small increase in temperature. However, the luminosity of the subgiant fit of model Z has luminosity halfway between that of model B and D. This means that if Collet et al. (2006) are correct the mass will need to be constrained to better than 0.025 $M_\odot$, in order to identify HE1327−2326 as a Population II or III star.

6 CONCLUSION

We have computed a series of stellar evolution models to help determine the origins of the HIP stars HE1327−2326 and HE0107−5240. In line with previous studies (Christlieb et al. 2004; Suda et al. 2004; Weiss et al. 2004), we find that the star HE0107−5240 appears to be a red giant or at least a subgiant close to the base of the red giant branch. Due to the uncertainties in the position of the red giant branch caused by the mixing-length treatment of superadiabatic convection, it is not possible to identify the position of HE0107−5240 on the giant branch. However, an accurate determination of the distance to HE0107−5240 would greatly help this situation.

Three proposed scenarios which give rise to the observed abundances of metals in HE1327−2326 have been tested. These scenarios are (i) a Population III star which has been enriched with metals by accretion from the interstellar medium, (ii) a secondary star of a Population III binary system which has been enriched by accretion from the primary star during its AGB phase, and (iii) an HIP star which formed with the abundances observed at the current epoch. We have tested two masses, 0.8 and 0.7 $M_\odot$, which give realistic age fits for subgiant and main-sequence stars, respectively. With the data currently available it is not possible to identify a favoured chemical enrichment scenario. As with the studies of Frebel et al. (2005) and Aoki et al. (2006) it has also not been possible to determine if HE1327−2326 is a main-sequence or subgiant star. However, if HE1327−2326 is a main-sequence star, then the luminosity and effective temperature of the ZAMS indicate it has mass less than about 0.8 $M_\odot$. If HE1327−2326 is assumed to around 12.5-Gyr old and to be a main-sequence star then it will have a mass closer to 0.7 $M_\odot$. If, however HE1327−2326 is a subgiant then the age of the best fit of 0.7-$M_\odot$ models is around 18 Gyr, which is considerably older than the *WMAP* estimate of the age of the Universe. This suggests that HE1327−2326 is likely to have a mass greater than 0.7 $M_\odot$, if it is a subgiant. At the age of best fit the main-sequence fits have accreted mass of the order of $10^{-3}\,M_\odot$ comprising 1 per cent metals by mass. The subgiant fits have far shallower convective envelopes, so have accreted only $\sim 10^{-5}\,M_\odot$ of matter at age of best fit. Both these values are several orders of magnitude larger than $2.6 \times 10^{-8}\,M_\odot$, which is the Suda et al. (2004) estimate for the total matter accreted from the interstellar medium over a 10-Gyr period, indicating that the gradual accretion scenario is unlikely. The recent differential study by Collet et al. (2006) suggest that the abundances of HE1327−2326 and HE0107−5240 need to be reduced by around an order of magnitude. This would require a proportionately smaller accretion rate, which at best, is still two orders of magnitude larger than the estimated rate of Suda et al. (2004).

The accretion of metals across the main sequence can allow a Population III star to approach the effective temperature and luminosity of comparable models for an HIP Population II star. The PP-chain is the dominant form of fusion across the main sequence. However, fusion via the CNO cycle is important on the subgiant and giant branches for stars which contain C, N and O. For stars with metal free cores, a higher core temperature is required to sustain fusion rates via the PP-chain. So subgiants with metal free cores have a luminosity about twice that of Population II subgiants. From ZAMS all the models computed here have radiative cores, as a result no significant quantities of C, N, O reach the core in any of the initially metal free accreting models.

If the distance to HE1327−2326 is measured, the resulting absolute magnitudes will allow it to be identified as a main sequence or a subgiant star. Furthermore, if HE1327−2326 is a subgiant star and its mass can be constrained to better than 0.05 $M_\odot$, it should be possible to determine if the star is Population II or III. However, if the metallicity suggested by Collet et al. (2006) for HE1327−2326 is correct, then mass would need to be constrained to better than 0.025 $M_\odot$.

ACKNOWLEDGMENTS

We thank the UK Particle Physics and Astronomy Research Council (PPARC) for financial support. We thank our anonymous referee for their constructive comments, which have helped to improve this paper.

REFERENCES

Angulo C. et al., 1999, Nucl. Phys. A, 656, 3
Aoki W., Norris J. E., Ryan S. G., Beers T. C., Ando H., 2002, ApJ, 567, 1166
Aoki W. et al., 2006, ApJ, 639, 897
Asplund M., Grevesse N., Sauval A. J., 2005, in Barnes T. G., III, Bash F. N., eds, ASP Conf. Ser. Vol. 336, Cosmic Abundances as Records of Stellar Evolution. Astron. Soc. Pac., San Francisco, p. 25
Barber R. J., Tennyson J., Harris G. J., Tolchenov R. N., 2006, MNRAS, 368, 1097
Bessell M. S., Christlieb N., Gustafsson B., 2004, ApJ, 612, L61
Bromm V., Loeb, 2003, Nat, 425, 812
Carbon D. F., 1974, ApJ, 187, 135
Cassisi S., Castellani V., Tornambe A., 1996, ApJ, 459, 298
Cayrel R., 2006, Rep. Prog. Phys., 69, 2823
Christlieb N. et al., 2002, Nat, 419, 904
Christlieb N., Gustafsson B., Korn A. J., Barklem P. S., Beers T. C., Bessell M. S., Karlsson T., Mizuno-Wiedner M., 2004, ApJ, 603, 708
Coc A., Vangioni-Flam E., Descouvemont P., Adahchour A., Angulo C., 2004, ApJ, 600, 544
Collet R., Asplund M., Trampedach R., 2006, ApJ, 644, L121
Dulick M., Bauschlicher C. W., Jr, Burrows A., Sharp C. M., Ram R. S., Bernath P., 2003, ApJ, 594, 651
Fitzpatrick E. L., 1999, PASP, 111, 63
Frebel A. et al., 2005, Nat, 434, 871
Goorvitch D., 1994, ApJS, 95, 535
Grevesse N., Noels A., Sauval A. J., 1996, in Holt S. S., Sonneborn G., eds, ASP Conf. Ser. Vol. 99, Cosmic Abundances. Astron. Soc. Pac., San Francisco, p. 117

Gustafsson B., Bell R. A., Eriksson K., Nordlund Å., 1975, A&A, 546, 407
Harris G. J., Polyansky O. L., Tennyson J., 2002, ApJ, 578, 657
Harris G. J., Lynas-Gray A. E., Miller S., Tennyson J., 2004a, ApJ, 600, 1025
Harris G. J., Lynas-Gray A. E., Miller S., Tennyson J., 2004b, ApJ, 617, L143
Harris G. J., Tennyson J., Kaminsky B. M., Pavlenko, Ya. V., Jones H. R. A., 2006a, MNRAS, 367, 400
Harris G. J., Lynas-Gray A. E., Tennyson J., Miller S., 2006b, in Lamers H., Langer N., Nugis T., Annuk K., eds, ASP Conf. Ser. Vol. 353, Stellar Evolution at Low Metallicity: Mass Loss, Explosions and Cosmology. Astron. Soc. Pac., San Francisco, p. 83
Harris G. J., Lynas-Gray A. E., Miller S., Tennyson J., 2007, MNRAS, 374, 337
Hubbard W. B., Lampe M., 1969, ApJS, 18, 297
Iglesias C. A., Rogers F. R., 1996, ApJ, 464, 943
Jørgensen U. G., Larsson M., 1990, A&A, 238, 424
Jørgensen U. G., Larsson M., Iwamae A., Yu B., 1996, A&A, 315, 204
Karlsson T., 2005, A&A, 439, 93
Karlsson T., 2006, ApJ, 641, L41
Kurucz R. L., 1995, in Sauval A. J., Blomme R., Grevesse N., eds, ASP Conf. Ser. Vol. 81, Laboratory & Astronomical High Resolution Spectra. Astron. Soc. Pac., San Francisco, p. 583
Luck R. E., 1993, in Sasselov D. D., ed., ASP Conf. Ser. Vol. 45, The Chemical Composition of Luminous High Latitude Post-AGB Stars in Luminous High-Latitude Stars. Astron. Soc. Pac., San Francisco, p. 87
Michaud G., Proffitt C. R., 1993, in Baglin A., Weiss W. W., eds, ASP Conf. Ser. Vol. 40, IAU Coll. 137, Inside the Stars. Astron. Soc. Pac., San Francisco, p. 246
Morel P., 1997, A&AS, 124, 597
Nakamura F., Umemura M., 2001, ApJ, 548, 19
Norris J. E., Ryan S. G., Beers T. C., 1997, ApJ, 489, L169
Plez B., 1998, A&A, 337, 495
Rogers F. J., Nayfonov A., 2002, ApJ, 576, 1064
Schlattl H., Salaris M., Cassisi S., Weis A., 2002, A&A, 395, 77
Suda T., Aikawa M., Machida M. N., Fujimoto M. Y., Iben I., 2004, ApJ, 611, 476
Weiss A., Schlattl H., Salaris M., Cassisi S., 2004, A&A, 422, 217

This paper has been typeset from a TEX/LATEX file prepared by the author.